

Non-Gaussianity and Non-Stationarity in Vibration Fatigue

Massimiliano Palmieri^a, Martin Česnik^b, Janko Slavič^{b,*}, Filippo Cianetti^a,
Miha Boltežar^b

^a*University of Perugia, Department of Engineering, via G. Duranti 93, 06125 Perugia, Italy*

^b*University of Ljubljana, Faculty of Mechanical Engineering, Aškerčeva 6, 1000 Ljubljana, Slovenia*

1. Highlights

- Theoretical and experimental research on non-Gaussianity and non-stationarity excitation.
- High-cycle fatigue of flexible structures excited close to natural frequencies.
- Non-stationarity excitation significantly impacts the fatigue life.
- Non-stationary vs non-Gaussian excitation were found much more important.

*Corresponding author. Tel.: +386 14771 226.
Email address: janko.slavic@fs.uni-lj.si

1
2
3
4
5
6
7
8
9
10
11
12
13
14
15
16
17
18
19
20
21
22
23
24
25
26
27
28
29
30
31
32
33
34
35
36
37
38
39
40
41
42
43
44
45
46
47
48
49
50
51
52
53

Non-Gaussianity and Non-Stationarity in Vibration Fatigue

Massimiliano Palmieri^a, Martin Česnik^b, Janko Slavič^{b,*}, Filippo Cianetti^a,
Miha Boltežar^b

^a*University of Perugia, Department of Engineering, via G. Duranti 93, 06125 Perugia,
Italy*

^b*University of Ljubljana, Faculty of Mechanical Engineering, Aškerčeva 6, 1000
Ljubljana, Slovenia*

Abstract

In vibration fatigue, flexible structures operate at or close to their natural frequencies. Therefore, it is common to consider the input excitation as well as the stress/strain response of the structure to be Gaussian and stationary. In reality, a non-Gaussian and non-stationary excitation is frequently observed, resulting in a possibly non-Gaussian and non-stationary response. The importance of this non-Gaussianity (typically observed via the kurtosis) has resulted in significant research on the relevance of the Gaussian assumption in fatigue life. For dynamic structures the prior research was mainly theoretically and numerically focused. This work researches the importance of non-Gaussianity and non-stationarity theoretically, numerically and experimentally. Y-shaped specimens were used in this research. The excitation close to the natural frequency is random and in all the researched cases with the same power spectral density (PSD). While the PSD was kept the

*Corresponding author. Tel.: +386 14771 226.
Email address: janko.slavic@fs.uni-lj.si

1
2
3
4
5
6
7
8
9 same, the rate of non-Gaussianity and the non-stationarity were changed.
10 The results show that when the excitation is stationary and non-Gaussian,
11 the fatigue life is not significantly impacted, and that standard frequency-
12 counting methods are applicable. However, for the case of a non-stationary,
13 non-Gaussian excitation, the fatigue life was found to be significantly im-
14 pacted and the Gaussian theoretical approach is questionable.
15
16
17
18
19

20 *Keywords:* Vibration fatigue testing, Fatigue parameters, Dynamic
21 excitation, Non-Gaussian stresses, kurtosis
22
23
24

25 **1. Introduction**

26
27
28 With the design of lighter and load-optimized products, random vibration
29 loads can significantly affect the fatigue life of flexible structures operating
30 close to their natural frequencies. This is known as vibration fatigue and has
31 been the subject of several research studies in recent years. In most cases,
32 it is common to assume a Gaussian distribution [1, 2] of both the input ex-
33 citation and the stress response. To estimate the fatigue life of a Gaussian
34 process, two approaches are available: the time domain and the frequency
35 domain [3, 4]. In the time domain the number of cycles as a function of the
36 stress amplitude (*i.e.*, fatigue loading spectrum) is estimated using the cycle-
37 counting method(*e.g.*, rainflow counting method) [3, 4, 5]. The cumulative
38 fatigue damage is then determined using the PalmgrenMiner rule with an SN
39 curve [3].
40
41
42
43
44
45
46
47
48
49
50

51 Alternatively, the cycle-counting and fatigue-damage analysis can be per-
52 formed using frequency-domain methods, which develop analytical formulas
53 from the process using its power spectral density (PSD) function. Several
54
55
56
57
58

1
2
3
4
5
6
7
8
9 frequency methods for cycle-counting are available in the literature. One of
10 the most widely used empirical formulas was proposed by Dirlik [6]. Fur-
11 thermore, an innovative counting method, used in this work, was found by
12 Benasciutti [7]; this gives the most accurate results relative to the rainflow
13 counting method [8].
14
15
16
17

18
19 In a real case, however, it is common to experience non-Gaussian load-
20 ings, and this can cause the response to be non-Gaussian, which may result
21 in a shorter fatigue life and for this reason, non-Gaussianity has been sub-
22 ject of several researches[9]. Some examples of non-Gaussian loads include
23 rail irregularities in rail ways and pressure fluctuations for the aerospace
24 sector. Particularly in the design and analysis of space shuttles and other ve-
25 hicles, there is a need to deal with the excitation processes as non-Gaussian.
26 Specifically, military environmental standards[10, 5] require a consideration
27 of the non-Gaussian behavior in simulation and testing environments. Sev-
28 eral studies have been published in recent years to understand the influence
29 of non-Gaussian excitation on the vibration fatigue life. Rizzi et al. [11],
30 Kihm et al. [12] and Niesłony et al. [13] investigated how non-Gaussian
31 excitation affects the fatigue life of linear and non-linear structures.
32
33

34 Otherwise, Braccesi et al. [14] investigated the possibility of correcting the
35 damage identified with the Gaussian-loads hypothesis by adopting a correc-
36 tive coefficient that they obtained as a function of non-Gaussian parameters
37 such as the kurtosis and skewness.
38
39
40
41
42
43

44 It has been numerically demonstrated that for a dynamic linear system
45 operating close to the natural frequency, the non-Gaussian excitation results
46 in a Gaussian response when the period of the systems impulse response
47
48
49
50
51
52
53
54
55
56
57
58

1
2
3
4
5
6
7
8
9 is much greater than the rate of the peaks in the loading. Instead, for a
10 non-linear system, the response to Gaussian or non-Gaussian excitations was
11 always non-Gaussian due to the violation of the central limit theorem [1].
12 Rizzi and Kihm obtained results for the case of kinematically excited struc-
13 tures.
14
15
16
17

18 Since the influence of the Gaussianity has been demonstrated, especially
19 with a numerical approach [11, 12, 14], the main aim of this study is to
20 experimentally research the influence of the non-Gaussianity on the fatigue
21 life of an actual structure and to certify whether and under what conditions
22 it is correct to adopt standard counting methods [6, 7] for the case of non-
23 Gaussian excitations. Since the studies [11, 12] numerically researched how
24 non-Gaussianity might affect the fatigue life, the influence of kurtosis on the
25 fatigue life is experimentally verified with several dynamic excitation.
26
27
28
29
30
31
32
33

34 In the present study three different types of random excitation signals
35 were generated from the PSD spectrums of constant shape *i.e.* stationary
36 Gaussian, stationary non-Gaussian and non-stationary non-Gaussian signal
37 type. For particular excitation type further variations were made by vary-
38 ing kurtosis and RMS amplitudes of signals. In detail, the specimens were
39 first tested under Gaussian conditions in order to estimate the material's
40 fatigue parameters. Once these characteristics were known, the influence of
41 the kurtosis was investigated by exciting the structure with non-Gaussian
42 random signals. A comparison between the actual and the estimated fatigue
43 life was carried out to understand under what circumstances it is appro-
44 priate to treat a random, non-Gaussian excitation as Gaussian, obtaining
45 results comparable to reality. As concerns this step, the fatigue life under
46
47
48
49
50
51
52
53
54
55
56
57
58

1
2
3
4
5
6
7
8
9
10
11
12
13
14
15
16
17
18
19
20
21
22
23
24
25
26
27
28
29
30
31
32
33
34
35
36
37
38
39
40
41
42
43
44
45
46
47
48
49
50
51
52
53
54
55
56
57
58
59
60
61
62
63
64
65

non-Gaussian excitations was estimated by using the corrective coefficient of non-Gaussianity proposed by Braccesi et al. [14].

This manuscript is organized as follows. In Section 2 the theoretical background of random signal properties and the different approaches to calculate the response of the dynamic structure are presented. Additionally, the frequency based, cycle-counting methods adopted in this work are shown. In Section 3 the experimental setup and the numerical model are presented. The results obtained from the Gaussian excitation are followed by the non-Gaussian results. Furthermore, a discussion regarding the effect of non-Gaussianity is presented. Section 4 draws the conclusions.

2. Theoretical Background

In order to control the vibration-fatigue phenomenon and the consequences that may result, several theoretical aspects of signal processing, the dynamic response of the structures and damage accumulation are required. In this section, the theoretical concepts used in this work are presented. Random signals are described with several parameters and only a complete knowledge of them allows us to understand the changes and behavior of the treated processes. Moreover, when a dynamic system is excited in the frequency range of its dynamic response the system's deflections amplify according to its natural frequencies and deflection modal matrix. Considering system's inherent strain modal matrix [15, 16] and strain-stress relations also system's stress amplifications can be observed and used to determine the stress-load at the areas of interest. Once the stress in the fatigue zone is known the damage accumulation can be determined with the different

1
2
3
4
5
6
7
8
9 methods available in the literature[17].

10 11 12 *2.1. Random Signal Properties*

13
14 A generic signal may belong to two macro categories: deterministic or
15 random. A deterministic signal is one where its value is known exactly at
16 every moment. Generally, in vibration analysis, engineers have to deal with
17 random signals. Since these random processes are time dependent, they can
18 only be treated using a probabilistic approach [1]: knowing the probability
19 of the fluctuation of a random signal, it is possible to acquire essential infor-
20 mation about the process itself.

21
22 A random process can be stationary or non-stationary, Gaussian or non-
23 Gaussian. A random variable x is said to be Gaussian if its probability
24 density function $P(x)$ (PDF) is given by:
25
26

$$27 \quad P(x) = \frac{1}{\sqrt{2\pi\sigma^2}} e^{-\frac{(x-\mu)^2}{2\sigma^2}}, \quad (1)$$

28
29 where μ is the mean value and σ is the standard deviation. The variance
30 σ^2 is the second central moment of $P(x)$, namely M_2 [4, 18]. For discrete
31 time-series data, the j -th central moment M_j and the mean μ are defined as:
32
33

$$34 \quad M_j = \frac{1}{n} \sum_{i=1}^n (x_i - \mu)^j, \quad (2)$$

$$35 \quad \mu = \frac{1}{n} \sum_{i=1}^n x_i, \quad (3)$$

36
37 where n is the number of points in the samples time history record. The
38 number of degrees of freedom for a given type of distribution is defined by
39
40
41
42
43
44
45

1
2
3
4
5
6
7
8
9 the number of moments required for its unique description [18]. For example,
10 with a Gaussian distribution, only two moments, the mean value μ and vari-
11 ance σ^2 suffice for a complete definition of the shape of the PDF; therefore, a
12 Gaussian distribution exhibits two degrees of freedom. Obviously, if a distri-
13 bution does not have a finite number of degrees of freedom, its definition will
14 become increasingly accurate as the order of its known moments increases.
15
16
17
18
19

20 A real random process may not follow a Gaussian normal distribution.
21 Two parameters, namely, the kurtosis k_u and the skewness s_k , are the prin-
22 cipal metrics describing the non-Gaussian features of the PDF. They may be
23 expressed in terms of the central moments as:
24
25
26
27
28
29

$$30 \quad k_u = \frac{M_3}{M_2^{3/2}} = \frac{M_3}{\sigma^3}, \quad s_k = \frac{M_4}{M_2^2} = \frac{M_4}{\sigma^4}. \quad (4)$$

31
32
33

34 The kurtosis characterizes the sharpness of the PDF peak and the width of
35 the PDF tails. The skewness is a measure of the asymmetry of the PDF.
36 A process is regarded as leptokurtic if its kurtosis is higher than 3, and
37 platykurtic if it is smaller than 3 [4].
38
39
40
41

42 Both kurtosis and skewness affect the damage-accumulation rate and con-
43 sequently the fatigue life. Indeed, under the hypothesis of a random, uni-axial
44 stress state, a process distribution with $k_u > 3$ determines a fatigue dam-
45 age higher than the Gaussian stress history, because the longer tails cause
46 fatigue cycles with a greater amplitude [7, 14]. In this study, the main focus
47 is given to the kurtosis value of the excitation and the stress response, since
48 it was shown [14] that the influence of the kurtosis is much higher than the
49 skewness.
50
51
52
53
54
55
56
57
58
59
60
61
62
63
64
65

1
2
3
4
5
6
7
8
9 *2.2. Structural Dynamics of Flexible Structures*

10 Flexible structures are, in structural dynamics, regarded as multi-degree-of-
11 freedom systems. In the case of dynamic excitation, the equation of motion
12 can be written as:
13
14
15

$$16 \quad \mathbf{M}\ddot{\mathbf{x}} + \mathbf{C}\dot{\mathbf{x}} + \mathbf{K}\mathbf{x} = \mathbf{f}, \quad (5)$$

17 where \mathbf{M} , \mathbf{C} and \mathbf{K} are the mass, damping and stiffness matrix, respectively.
18 Vector \mathbf{x} represents the displacement of the system's degrees of freedom,
19 while the vector \mathbf{f} represents the force as the input to the system. In order
20 to describe dynamic body behavior, the modal approach is widely used in
21 structural dynamics [19] and allows us to write the equation of motion in an
22 alternative form as:
23
24
25
26
27
28
29
30
31

$$32 \quad \mathbf{I}\ddot{\mathbf{q}} + [\mathbf{2}\xi\omega_0]\dot{\mathbf{q}} + [\omega_0^2]\mathbf{q} = \mathbf{\Phi}^T\mathbf{f}, \quad (6)$$

33 where:

$$34 \quad \mathbf{x} = \mathbf{\Phi}\mathbf{q}. \quad (7)$$

35 Equation 6 is the equation of motion for the system in terms of the normalized
36 coordinates \mathbf{q} . In this equation \mathbf{I} represents the identity matrix, $[\mathbf{2}\xi\omega_0]$
37 is the damping matrix and $[\omega_0^2]$ is the diagonal matrix of the eigenvalues
38 obtained due to the modal analysis. The deformations are estimated through
39 a displacement function obtained by multiplying the shape function $\mathbf{\Phi}$ and
40 the generalized coordinates \mathbf{q} . The stress state of the dynamic structure can
41 be reconstructed using:
42
43
44
45
46
47
48
49
50
51
52

$$53 \quad \sigma_{ij} = \sum_{k=1}^m \Phi_{ij,k}^s q_k, \quad (8)$$

1
2
3
4
5
6
7
8
9 where σ_{ij} represents the time history of the stress-tensor component with i
10 and j referred to the stress-tensor indices, m is the number of modal coor-
11 dinates, \mathbf{q}_k is the k -th generalized coordinate time history and $\Phi_{ij,k}^s$ is the ij
12 component of the k -th stress modal shape function. The system response can
13 be evaluated by a superposition of the response of one-degree-of-freedom sys-
14 tems (modal coordinates), each multiplied by a constant (the related modal
15 shapes).

16
17 Using the hypothesis of a linear time-invariant system, it is also possible
18 to obtain the representation in the frequency domain of the state of stress
19 for a component starting from the input PSD matrix [20, 21]. With the lin-
20 earization of a state-space model, assuming a known excitation as the input
21 and the generalized coordinates \mathbf{q} as the output of the flexible component,
22 it is possible to obtain the PSD matrix \mathbf{S} of the stress as shown in Eq.(9)
23
24
25
26
27
28
29
30
31
32
33
34

$$35 \quad \mathbf{S} = \Phi^s [\mathbf{H}_q^* \mathbf{G}_x \mathbf{H}_q^T] \Phi^{s^T}. \quad (9)$$

36
37 The modal matrix of the modal shapes Φ^s is multiplied by the product of
38 the matrix of the frequency-response function \mathbf{H}_q and the generic PSD of the
39 excitation given as a matrix of n inputs \mathbf{G}_x , to obtain the power spectrum
40 density matrix \mathbf{S} of the stress. \mathbf{H}_q is the matrix of the frequency-response
41 functions ($m \times n$) between n generic inputs and the m generalized coordi-
42 nates as outputs. \mathbf{H}_q represents, in the frequency domain, the contribution
43 of the individual generalized coordinates to the deformation of the flexible
44 component. The symbols $*$ and T denote the complex conjugate and the
45 transposed matrix, respectively. Once the stress PSD matrix to the random
46 dynamic excitation is obtained for an arbitrary point of the structure, a fa-
47
48
49
50
51
52
53
54
55
56
57
58
59
60
61
62
63
64
65

1
2
3
4
5
6
7
8
9 tigue analysis can be performed.

10
11 To perform a fatigue analysis for the multi-axial stress state in the fre-
12
13 quency domain, different methods are available in the literature [22]. Here it
14
15 is necessary to compute the PSD matrix of the equivalent von Mises stress
16
17 [23, 24] in the frequency domain:
18
19

$$20 \mathbf{S}_{\text{eq}}(\omega) = \text{Trace}[\mathbf{Q}\mathbf{S}(\omega)]. \quad (10)$$

21
22
23 In Eq.(10), \mathbf{Q} is a constant matrix, which for a planar stress state is given
24
25 by:
26
27

$$28 \mathbf{Q} = \begin{bmatrix} 1 & -1/2 & 0 \\ -1/2 & 1 & 0 \\ 0 & 0 & 3 \end{bmatrix}. \quad (11)$$

29
30
31
32
33
34 Using this definition, the equivalent von Mises stress is a stationary zero-
35
36 mean Gaussian process[23, 24]; therefore, the existing frequency methods for
37
38 the fatigue-life calculation can be used.
39
40

41 *2.3. Fatigue Damage Accumulation*

42
43 The fatigue life can be estimated in the time domain or the frequency do-
44
45 main. In general, the frequency-domain approach is a privileged domain for
46
47 the observation and analysis of random excitation of a dynamic structure.
48
49 In fact, a random process can be efficiently defined by its power spectral
50
51 density, which represents the power distribution along the frequency content
52
53 of the process. Whichever frequency-counting method is used, the spectral
54
55 moments should be known [3]. The shape of the equivalent stress PSD $\mathbf{S}_{\text{eq}}(\omega)$
56
57
58
59
60
61
62
63
64
65

Eq.(10), can be characterized with a set of spectral moments; for a stationary and a zero mean valued random process, the m -th moment is defined as:

$$\lambda_m = \int_0^\infty \omega^m \mathbf{S}_{\text{eq}}(\omega) d\omega. \quad (12)$$

Certain spectral moments of the equivalent stress PSD $\mathbf{S}_{\text{eq}}(\omega)$ can be used to describe the key properties of a stress loading in the time domain. The number of zero crossings with a positive slope ν_0 per unit time and the expected rate of occurrence of the peaks ν_p are defined as [7]:

$$\nu_0 = \frac{1}{2\pi} \sqrt{\frac{\lambda_2}{\lambda_0}}, \quad \nu_p = \frac{1}{2\pi} \sqrt{\frac{\lambda_4}{\lambda_2}}. \quad (13)$$

A spectral density $\mathbf{S}_{\text{eq}}(\omega)$ can also be described by bandwidth parameters; the most commonly used are:

$$\alpha_1 = \frac{\lambda_1}{\sqrt{\lambda_0 \lambda_2}}, \quad \alpha_2 = \frac{\lambda_2}{\sqrt{\lambda_0 \lambda_4}}. \quad (14)$$

The damage calculation arises from the assumption of the linear damage-accumulation law of Palmgren-Miner [3]. Under such conditions, the total damage can be determined as:

$$D = \sum_i \frac{n_i}{N_i}, \quad (15)$$

where D denotes the total fatigue damage, n_i denotes the number of cycles under a certain stress amplitude and N_i is the total number of cycles to failure associated with the stress amplitude. The fatigue failure occurs when the damage D achieves the value 1. The number of cycles n_i depends on the material fatigue properties, which are described with Basquin's equation[25]:

$$\sigma = CN^{-1/b}, \quad (16)$$

where σ represents the stress amplitude and N is the number of cycles to the fatigue failure. The C and b shown in Eq.(16) are referred to the fatigue strength and fatigue exponent, respectively. Introducing Eq.(16) into Eq.(15), the damage intensity can be expressed as:

$$D = \frac{1}{2\pi} C^{-b} \nu_p \int_0^\infty \sigma^b p_a(\sigma) d\sigma, \quad (17)$$

where p_a denotes the amplitude distribution of the load time history. In a random process, the amplitude is a random variable, and thus the damage D is a random variable as well. From Eq.(16) it is clear how the damage intensity is correlated to the b -th moment of the stress-amplitude distribution.

Alternatively, the frequency-domain approach is only based on the characteristics of the equivalent stress PSD $\mathbf{S}_{\text{eq}}(\omega)$ and on the fatigue properties of the material. In this work the Tovo-Benasciutti method is used [7], since it was shown by [8] that it provides better results than other methods in the frequency domain. The Tovo-Benasciutti method is a combination of the Narrow-Band and the Range-Count counting methods, and for a strictly narrow-band Gaussian process, the fatigue-damage intensity can be written as:

$$D_{NB} = \alpha_2 \nu_p C^{-b} (\sqrt{2\lambda_0})^b \Gamma(1 + \frac{b}{2}). \quad (18)$$

The Tovo-Benasciutti counting method is related to the narrow-band counting method, as shown in the following formula:

$$D = (B_{tb} + (1 - B_{tb})\alpha_2^{B_{tb}-1})\alpha_2 D_{NB}. \quad (19)$$

where B_{tb} is a factor obtained from the bandwidth parameters of the stress PSD:

$$B_{tb} = \frac{(\alpha_1 - \alpha_2)(1.112(1 + \alpha_1\alpha_2 - (\alpha_1 + \alpha_2))e^{2.11\alpha_2} + (\alpha_1 - \alpha_2))}{(\alpha_2 - 1)^2}. \quad (20)$$

1
2
3
4
5
6
7
8
9 Here, α_1 and α_2 are the bandwidth parameters defined in Eq.(12).

10
11 The Tovo-Benasciutti method has only been validated for Gaussian exci-
12 tations. In the literature it is possible to find several methods that allow a
13 damage estimation under the hypothesis of non-Gaussianity. In general, the
14 use of cycle counting methods based on Gaussian excitations may simplify the
15 determination of the fatigue life, also in the case of non-Gaussian excitation.
16 In order to evaluate how the non-Gaussian excitations affect the fatigue life,
17 and thereby to be able to know when it is correct to adopt standard cycle-
18 counting methods for the case of non-Gaussian excitation, in this paper the
19 Tovo-Benasciutti counting method is used for both conditions: Gaussianity
20 and non-Gaussianity.
21
22
23
24
25
26
27
28
29

30 The adoption of a non-Gaussianity coefficient that corrects the damage
31 evaluation performed under the Gaussian-loads hypothesis is an alternative
32 approach that can be found in the literature [14]. This coefficient allows an
33 estimation of the fatigue life under non-Gaussian loadings using the Gaus-
34 sian approach. In fact, the damage caused by a non-Gaussian input D_{ng} can
35 be easily obtained just by multiplying the Gaussian damage D_g , which is
36 known if the PSD of the stress is known, for the corrective coefficient of non-
37 Gaussianity λ_{ng} [14, 26, 27]. In this manner, the damage for a non-Gaussian
38 input can be determined as follows:
39
40
41
42
43
44
45
46
47

$$48 \quad D_{ng} = \lambda_{ng} D_g. \quad (21)$$

49
50
51 The formula proposed by Braccesi et al.[14] for the non-Gaussian correc-
52 tive coefficient is used in this research:
53
54

$$55 \quad \lambda_{ng} = e^{\frac{m^{3/2}}{\pi} \left(\frac{(k_u-3)}{5} - \frac{s_k^2}{4} \right)}. \quad (22)$$

1
2
3
4
5
6
7
8
9 Eq.(22) has a compact form and simple dependencies on k_u, s_k and m . Com-
10 pared to the other formulas available in the literature [26, 27] the effect of
11 the stress RMS is ignored here. Keeping in mind that the focus of this
12 work is to understand how non-Gaussianity affects the fatigue life, the non-
13 Gaussianity coefficient is calculated and adopted only to understand whether
14 if it is correct to determine the accumulation damage in the condition of non-
15 Gaussianity, as in the Gaussian condition obtaining a realistic value.
16
17
18
19
20
21
22

23 **3. Experimental and Numerical Research**

24
25
26 The experimental part of this research begins with a series of stationary
27 Gaussian loadings where different types of random signal were studied. A
28 numerical model was used to obtain the material's parameters. With the
29 Gaussian experiments the fatigue parameters were known, and an additional
30 set of non-Gaussian experiments was performed.
31
32
33
34
35

36 A comparison between the experimental and numerical fatigue life was
37 performed to understand how the damage rate increases for the non-Gaussian
38 excitations when compared to the Gaussian excitation. At the end, a correc-
39 tive coefficient was computed to adjust the calculated fatigue life under the
40 conditions of non-Gaussianity.
41
42
43
44
45

46 *3.1. Experiment Setup*

47
48 In this research a Y-shaped specimen, shown in Fig. 1 was used [28, 29, 30].
49 Its geometry consists of three main beams that are arranged at 120° angles
50 around the main axis and have a rectangular cross-section of 10×10 mm.
51 The Y-shaped specimens were made from the aluminum alloy A-S8U3 by
52 casting and with the surface finish produced by milling. The fatigue zone
53
54
55
56
57
58

1
2
3
4
5
6
7
8
9 was additionally fine-ground in order to remove any scratches that could
10 cause the premature start of an initial crack. Additional steel dead-weights
11 with a mass of 52.5 g were added at the end of the two beams. These
12 masses were used to adjust the initial natural frequency of the Y-specimen.
13 The following material parameters of the aluminum were used: density of
14 $\rho = 2710 \text{ kg/m}^3$ and Young's modulus of $E = 75000 \text{ MPa}$. By evaluating the
15 dynamic response of the Y-shaped specimen (Table 1) the fourth-mode shape
16 at $\omega_4 = 775 \text{ Hz}$ was recognized as the most suitable for the near-resonance
17 fatigue test. For simplicity, the fourth natural frequency will be denoted as
18 ω_1 instead of ω_4 .
19
20
21
22
23
24
25
26
27

28 In the presented experimental setup, the Y-shaped specimen is attached
29 with a fixation adapter to the LDS V555 electro-dynamical shaker, as shown
30 in Fig.1. The excitation force was applied in form of a narrow-band random
31 signal with a flat PSD profile, as shown in Fig. 2. To ensure the correct
32 characteristics of the excitation force applied to the shaker's armature (*i. e.*
33 kurtosis, PSD function and RMS value), a preliminary experiment was per-
34 formed. There a specimen was removed from fixation adapter to prevent any
35 dynamic amplifications, a drive signal was applied to amplifier and an accel-
36 eration signal on fixation adapter was measured. The measured acceleration
37 was later multiplied with mass properties of all moving bodies to confirm
38 required excitation force characteristics.
39
40
41
42
43
44
45
46
47
48

49 As shown in Fig. 2, a PSD profile with frequency range from 600 Hz
50 to 850 Hz near the specimen's fourth natural frequency was proposed. The
51 selection of a narrow-band random profile in the vicinity of a single natural
52 frequency greatly reduces the influence of the remaining modes on the sys-
53
54
55
56
57
58
59
60
61
62
63
64
65

1
2
3
4
5
6
7
8
9 tem's dynamic response and damage accumulation. However, the frequency
10 band of the excitation should be wide enough to ensure an unaltered excita-
11 tion of the observed mode shape throughout the fatigue test, even when due
12 to the fatigue crack propagation a slight shift of the natural frequency shift
13 occurs.
14
15
16
17

18 In their studies, Rizzi et al. [11] numerically verified that the response
19 of a linear system to a stationary, non-Gaussian signal is always Gaussian
20 due to the central limit theorem. Instead, if the burst duration of a non-
21 stationary, non-Gaussian signal is comparable to the impulse response period
22 of the dynamic structure, the central limit theorem is not verified and the
23 response of the system is non-Gaussian [11]. Considering these conclusions,
24 three different types of signals were researched: stationary Gaussian, sta-
25 tionary non-Gaussian and non-stationary(burst) non-Gaussian. The signals
26 are shown in Fig. 3 and in Tab. 2. They all had the same PSD shape.
27 The stationary non-Gaussian signals were generated, as stated in Tab. 2,
28 for two different kurtosis values, 7 and 5.5, respectively, and show a sta-
29 tionary rate of high excursion peaks, while the burst non-Gaussian signal
30 presents a kurtosis of 7 and shows a burst of high-excursion peaks. In order
31 to generate the stationary, non-Gaussian signals, the method proposed by
32 [31, 32], which uses Hermite polynomials, was adopted in this work, while
33 the burst non-Gaussian signal was constructed following the same method
34 as used by Kihm et al. [12]: firstly a Gaussian stationary signal is generated
35 from the given PSD; secondly, a low-frequency carrying amplitude carrier
36 wave is constructed. The amplitudes of the generated wave are realizations
37 of a β distribution. Finally, the resulting signal is obtained by multiplying
38
39
40
41
42
43
44
45
46
47
48
49
50
51
52
53
54
55
56
57
58
59
60
61
62
63
64
65

1
2
3
4
5
6
7
8
9 both signals and then scaling to the original RMS value. As shown in Fig.
10 3, the Gaussian signal and the stationary, non-Gaussian signal have a time
11 duration of 7.5 seconds due to the stationarity. Indeed, since the stationary
12 signals are time independent, the statistical characteristics are known for
13 every time; therefore, it is possible to reduce the signal's duration without
14 losing any information. Instead, for the burst, non-Gaussian signal a longer
15 time duration is necessary. Since the generated signal in Fig. 3 d) is clearly
16 non-stationary, a longer time duration of 30 seconds was used to consider the
17 influence of every burst.
18
19
20
21
22
23
24
25

26 A total of 13 specimens were tested in this work. Four specimens were
27 excited with a stationary, Gaussian loading, six specimens with a stationary,
28 non-Gaussian loading (three with a kurtosis of 7 and three with a kurtosis
29 of 5.5) and three specimens with burst, non-Gaussian loadings. For details,
30 see Tab.3.
31
32
33
34
35

36 Additionally, to evaluate the actual kurtosis of the stress response a strain
37 gauge was also applied in the vicinity of the fatigue zone, as shown in Fig.1.
38 In this way, the time histories of the specific deformation and, consequently,
39 the stress time histories were obtained.
40
41
42
43

44 *3.2. Numerical Model*

45

46 The numerical analysis follows the approach stated in Sec. 2, but applied to
47 the dynamic response obtained with the finite-element method. Firstly, the
48 stress response PSD matrix is calculated for the given specimen geometry,
49 boundary conditions and applied random vibration profile. Secondly, the
50 equivalent stress PSDs are obtained for the elements of interest. Thirdly,
51 the statistical characteristics of the equivalent stress PSDs are calculated.
52
53
54
55
56
57
58

1
2
3
4
5
6
7
8
9
10
11
12
13
14
15
16
17
18
19
20
21
22
23
24
25
26
27
28
29
30
31
32
33
34
35
36
37
38
39
40
41
42
43
44
45
46
47
48
49
50
51
52
53
54
55
56
57
58
59
60
61
62
63
64
65

Lastly, by introducing the material's fatigue parameters and the statistical characteristics of the stress PSD into the damage-intensity equation, the expected fatigue life for a single element is obtained. As shown in Eq. (9), the determination of the frequency response function (FRF) is necessary. Since the FRF depends on the modal properties, *e.g.*, natural frequencies, damping factors and mode shapes, a finite-element model and, consequently, a modal analysis is required. For the Y-shaped specimen, the modal shapes and natural frequencies were calculated using a commercial FEM tool. The finite-element model consisted of 15600 10-node tetrahedral solid elements. Since the fatigue crack normally starts on an external surface and in order to reduce the calculation time, Shell63 skin elements, with a thickness of 1×10^{-6} mm were applied at the external and surface modal shapes of the displacement and the stresses were extracted only for these elements. The FEM model is shown in Fig. 4. Two inertial weights on the Y specimens were considered as two single points placed at the same position as the center of mass of the weights. In order to validate the numerical model, a comparison of the acceleration response PSD at the location denoted in Fig. 4 and the random force input was made for the numerical model and the actual specimen, Fig. 5. The presented numerical model's linear response coincides with the measured initial response of the actual specimen before a significant vibration load was applied. For the numerical calculation of damage accumulation rate the structure's modal parameters are assumed to be constant during the fatigue life. This assumption is justified when the excitation PSD profile is flat and of appropriate frequency width [28].

At the end, an additional numerical analysis in the time domain was

1
2
3
4
5
6
7
8
9 performed in order to compute the time history of the stress in the fatigue
10 zone, whose location is shown in Fig. 4. The kurtosis of the response was
11 calculated for each excitation signal. In this way a comparison between the
12 actual and the calculated kurtosis of the stress was carried out.
13
14
15
16

17 *3.3. Experiment with Gaussian Excitation*

18
19
20 As stated in Tab. 3 four different specimens (specimen no.1-4 in table 2)
21 were excited with a Gaussian excitation using three different PSD levels. The
22 fatigue crack initiated on the external surface, as expected, and was observed
23 by monitoring the natural frequency shift. This shift is a consequence of the
24 fatigue crack growth, see Fig. 6. Consequently, the final fatigue failure was
25 determined when the natural frequency reached 600Hz. This is in agreement
26 with the work of many authors [6, 17] who assume that the frequency shift
27 relates to the accumulated fatigue damage. Using the validated numerical
28 model and the input Gaussian excitation shown in Fig. 3a, the fatigue lives
29 were numerically determined with the Tovo-Benasciutti counting method [7]
30 for each level of amplitude of the loadings. The results are given in Tab.3.
31
32
33
34
35
36
37
38
39
40

41 Since the fatigue lives under Gaussian conditions were determined exper-
42 imentally, the fatigue parameters can be assessed by updating the numerical
43 model. When assessing the fatigue parameters with the Tovo-Benasciutti
44 frequency method, the damage intensity is not linearly related to the mate-
45 rial's fatigue parameters. Therefore, a numerical minimization of the sum of
46 the squared difference between the estimated and experimental fatigue lives
47 of the test specimens is used. Here, the function being minimized is written
48
49
50
51
52
53
54
55
56
57
58

1
2
3
4
5
6
7
8
9
10
11
12
13
14
15
16
17
18
19
20
21
22
23
24
25
26
27
28
29
30
31
32
33
34
35
36
37
38
39
40
41
42
43
44
45
46
47
48
49
50
51
52
53
54
55
56
57
58
59
60
61
62
63
64
65

as:

$$\Delta T(b, C) = \sum_i (\log_{10}(T_{act,i}) - \log_{10}(T_{est,i}(b, C)))^2, \quad (23)$$

where i denotes a single test specimen, T_{act} is the measured fatigue life of the specimen and T_{est} is the estimated fatigue life of the specimen based on the numerical model. The minimization method showed a strong convergence. Using the identified fatigue parameters, Basquin's equation (15) can be written as:

$$\sigma = 987.5 \cdot N^{-0.169}. \quad (24)$$

The obtained values in Eq. (24) for the fatigue strength C and the fatigue exponent b show a good correlation with the values obtained by Česnik et al. [28].

Fig. 7 shows a comparison between the actual fatigue life and the fatigue life calculated using the fatigue parameters in Eq. (23). The results of Tab. 3 are also shown in Fig. 7, where the calculated fatigue lives for the Gaussian and non-Gaussian stationary excitations show a good agreement with the actual lives, confirming the correctness of the numerical model. Since there is a good agreement between the experimental and calculated lives, it was necessary to test only 4 specimens.

3.4. Experiment with non-Gaussian Excitation

In this section the Y-shaped specimens were excited with non-Gaussian loadings until the fatigue failure occurred. Here, as shown in Fig. 3, two different non-Gaussian excitation types were considered (stationary and burst non-stationary, respectively, specimens no. 5–10 for stationary and no. 11–13 for

1
2
3
4
5
6
7
8
9 burst, Table 3). In order to obtain representative results for the leptokur-
10 tic condition, stationary signals with two different kurtosis, 7 and 5.5, were
11 used. Similar to the excitation with Gaussian signals, all the non-Gaussian
12 signals were generated with three different RMS amplitudes, but with the
13 same PSD shape, Table 3. A total of nine Y-shaped specimens were tested,
14 three for each excitation signal. In order to evaluate the influence of the
15 kurtosis on the fatigue life of the tested specimens, the fatigue parameters
16 obtained under the Gaussian condition are also used for a numerical estima-
17 tion of the fatigue life for the case of non-Gaussian excitation. In order to
18 investigate when it is justified to apply Gaussian-based counting methods to
19 a non-stationary excitation, the Tovo-Benasciutti counting method was also
20 used in the case of the non-Gaussian excitations.
21
22
23
24
25
26
27
28
29
30
31

32 The natural frequency shifts during the random excitation fatigue test
33 are shown in Fig. 6. From this we can see that the frequency shifts due
34 to the stationary non-Gaussian loadings, even if slightly faster, are compa-
35 rable to the shifts obtained due to the Gaussian loadings. Instead, faster
36 frequency shifts occur under the burst non-Gaussian excitation compared to
37 the Gaussian tests.
38
39
40
41
42

43 Therefore, a comparison between the experimental and calculated fatigue
44 lives is shown in Fig. 7. From Fig. 7 it is noticeable that the stationary,
45 non-Gaussian excitation differs only slightly if compared to the calculated
46 fatigue life. In contrast to this case, for the case of burst, non-Gaussian
47 excitation, the comparison shows how the difference between the calculated
48 fatigue lives and the actual fatigue lives is significant. From this comparison
49 we can conclude that for the case of stationary excitation the use of stan-
50
51
52
53
54
55
56
57
58
59
60
61
62
63
64
65

1
2
3
4
5
6
7
8
9 dard frequency-counting methods [3] available in the literature gives reliable
10 results comparable to reality, while in the case of strongly non-stationary sig-
11 nals the use of the same counting methods supplies uncorrected results. The
12 Figure 8 shows the relation between the excitation force PSD amplitude and
13 the experimental fatigue life; again, the non-stationary experiments clearly
14 differentiate from the stationary experiments.
15
16
17
18
19

20 The significant difference between the calculated and measured fatigue
21 lives in the case of burst, non-stationary excitations arises due to the non-
22 Gaussianity of the stress response. For this reason a piezo-electric strain
23 gauge was applied on the specimen beam, as shown in Fig.1, to monitor the
24 deformation and the stress response. The kurtosis of the stress response was
25 experimentally obtained for each test case and it is stated in Tab.4. For the
26 case of stationary non-Gaussian loadings the kurtosis of the stress is always
27 around the value 3, confirming that due to the stationarity of the excitation,
28 the response of the structure is Gaussian. However, for the case of burst,
29 non-Gaussian loadings the output kurtosis is significantly higher, although
30 it is still lower than the kurtosis of the input signal. In any case we can con-
31 clude that if the input signal is quasi-stationary, the output kurtosis always
32 tends to the Gaussianity; however, if the input signal is non-stationary, the
33 stress response remains strongly non-Gaussian.
34
35
36
37
38
39
40
41
42
43
44
45
46

47 Furthermore, a time-domain analysis was also carried out to numerically
48 determine the stress-response kurtosis for the observed non-Gaussian excita-
49 tion signals. As stated in Tab.4, the kurtosis of the stress response is compa-
50 rable to the actual measured value. Based on the obtained stress response,
51 the non-Gaussianity coefficient was numerically determined to compare the
52
53
54
55
56
57
58
59
60
61
62
63
64
65

1
2
3
4
5
6
7
8
9 estimated fatigue lives to the actual fatigue lives. As stated in Tab.5 and
10 shown in Fig. 9, it is evident that in the case of the stationary non-Gaussian
11 signal, the correction coefficient gives a value close to the unit, while in the
12 case of a non-stationary signal the value of the corrective coefficient is larger
13 than ten. On one hand this confirms how stationary excitations do not sig-
14 nificantly affect the fatigue lives; meanwhile, on the other hand, an increase
15 in the damage occurs if the structure is exposed to burst, non-stationary
16 excitations. For this reason, it is reasonable to affirm that for the case of
17 stationary, non-Gaussian excitation, frequency-counting methods, confirmed
18 only for Gaussian conditions, can be adopted and that the resulting error can
19 be neglected. Instead, if the input non-Gaussian excitation is strongly non-
20 stationary the approximation obtained by considering non-Gaussian signals
21 as Gaussian leads to substantial errors in the damage calculation.
22
23
24
25
26
27
28
29
30
31
32
33
34

35 **4. Conclusions**

36
37
38 In the presented research the fatigue life of a simple Y-shaped specimen
39 was investigated in order to determine how a change in the excitation kurtosis
40 affects the fatigue life of a real structure. To this end, several experimental
41 verifications of random excitation signals with the same PSDs, but with dif-
42 ferent kurtosis were performed. In the case of stationary random excitations,
43 it was found that non-Gaussian signals with a stationary rate of high excur-
44 sion peaks produced a Gaussian response, while in the case of non-stationary
45 random signals, the response of the structure is non-Gaussian. The obtained
46 results show that the fatigue life due to burst, non-stationary excitations is
47 significantly shorter when compared to the fatigue lives obtained under the
48
49
50
51
52
53
54
55
56
57
58
59
60
61
62
63
64
65

1
2
3
4
5
6
7
8
9 condition of stationarity. Due to the results obtained in this research, it is
10 reasonable to state that even if it is common in engineering practice, the
11 approximation to consider a non-Gaussian excitation as Gaussian does not
12 always produce accurate results. Moreover, it was found that if the non-
13 Gaussian excitation is stationary, the calculated fatigue lives with classical
14 frequency-counting methods are comparable to the fatigue lives under Gaus-
15 sian excitation; therefore, justifying the use of frequency-counting methods,
16 even if validated only in the case of Gaussian excitations. In contrast, for
17 the case of burst, non-Gaussian excitation, the obtained fatigue life exhibits
18 a significantly higher damage accumulation compared to the fatigue lives at-
19 tained under Gaussian signals. For this reason, considering a non-stationary
20 non-Gaussian excitation as Gaussian and, consequently adopting the classic
21 frequency-counting methods may result in a wrong fatigue-life estimation.
22 This fatigue-life reduction can be justified as a result of high peak excursions
23 observed during burst non-stationary excitation, that are required to main-
24 tain the required RMS value and PSD profiles of the excitation acceleration.
25 These peaks consequently alter the stress-load spectrum from Gaussian to
26 non-Gaussian with higher rate of high-amplitude cycles. Relating to the ex-
27 isting studies that are dealing with external force loads, the non-Gaussian
28 stress-load spectrum results in a shorter fatigue life.

29
30
31
32
33
34
35
36
37
38
39
40
41
42
43
44
45
46
47 Further confirmation about the probability distribution of the response
48 arises from additional tests. A piezo-electric strain gauge made it possible
49 to investigate the kurtosis of the stress response in the fatigue zone. It was
50 found experimentally that in the case of stationary excitations, the kurtosis
51 of the response tends to three, while in the case of burst, non-stationary sig-
52
53
54
55
56
57
58
59
60
61
62
63
64
65

1
2
3
4
5
6
7
8
9
10
11
12
13
14
15
16
17
18
19
20
21
22
23
24
25
26
27
28
29
30
31
32
33
34
35
36
37
38
39
40
41
42
43
44
45
46
47
48
49
50
51
52
53
54
55
56
57
58
59
60
61
62
63
64
65

nals the output kurtosis is higher. This confirms how in the case of strongly non-stationary excitations, the structure transfers the characteristic of the input signal and for this reason the obtained fatigue life is definitely shorter than in the case of Gaussian or stationary, non-Gaussian excitations.

Acknowledgment

The authors acknowledge the partial financial support from the Slovenian Research Agency (research core funding No. P2-0263 and project L2-6772).

1
2
3
4
5
6
7
8
9
10
11
12
13
14
15
16
17
18
19
20
21
22
23
24
25
26
27
28
29
30
31
32
33
34
35
36
37
38
39
40
41
42
43
44
45
46
47
48
49
50
51
52
53
54
55
56
57
58
59
60
61
62
63
64
65

References

- [1] S. Bendat and G. Piersol. *Random data: analysis and measurement procedures*. WILEY, 4th edition, 2010.
- [2] S. Bendat. Probability functions for random responses: Prediction of peaks, fatigue damage, and catastrophic failures. 1964. Contract No. NAS-5-4590.
- [3] Y. L. Lee, J. Pan, R. B. Hathaway, and M. E. Barkey. *Fatigue Testing and Analysis: Theory and Practice*. Elsevier, Oxford, UK, 1st edition, 2005.
- [4] D. E. Newland. *An introduction to Random vibration and spectral analysis*. Longmann Scientific and Technical, Essex, England, 2nd edition, 1984.
- [5] Defense Standard 00-35. Environmental handbook for defense material. part 5: Induced mechanical environments. 1999.
- [6] T. Dirlik. *Application of computer in fatigue analysis*. PhD thesis, University of Warwick, 1985.
- [7] D. Benasciutti. *Fatigue analysis of random loadings*. PhD thesis, University of Ferrara, 2004.
- [8] M. Mršnik, J. Slavič, and M. Boltežar. Frequency-domain methods for a vibration-fatigue-life estimation - application to real data. *International Journal of Fatigue*, 47:8–17, 2013.

- 1
2
3
4
5
6
7
8
9 [9] P. Wolfsteiner. Fatigue assessment of non-stationary random vibrations
10 by using decomposition in gaussian portions. In *International Journal of*
11 *Mechanical Sciences*, University of Applied Sciences Munich, Dachauer
12 Straße 98B, 80335 München, Germany, 2016.
13
14
15
16
17 [10] MIL-STD-810F. Department of defense test method standard for en-
18 vironmental engineering consideration and laboratory tests. January
19 2000.
20
21
22
23 [11] S. A. Rizzi, A. Prezekop, and T. Turner. On the response of a
24 non-linear structure to high kurtosis non-gaussian random loadings.
25 *EURODYN2011- 8th International Conference on Structural Dynamics;*
26 *Leuven; Belgium*, 2011.
27
28
29
30
31
32 [12] F. Kihm, S. A. Rizzi, N. S. Ferguson, and A. Halfpenny. Understanding
33 how kurtosis is transferred from input acceleration to stress response
34 and its influence on fatigue life. *RASD*, 11th International Conference,
35 July 2013.
36
37
38
39
40 [13] A. Niesłony, M. Bohm, T. Lagoda, and F. Cianetti. The use of spectral
41 method for fatigue life assessment for non-gaussian random loads. *Acta*
42 *Mechanica et Automatica*, 10(2):100–103, 2016.
43
44
45
46
47 [14] C. Braccési, F. Cianetti, G. Lori, and D. Pioli. The frequency domain
48 approach in virtual fatigue estimation of non-linear system: the prob-
49 lem of non-gaussianity state of stress. *International Journal of Fatigue*,
50 31(4):766–775, 2009.
51
52
53
54
55
56
57
58

- 1
2
3
4
5
6
7
8
9 [15] T. Kranjc, J. Slavič, and M. Boltežar. A comparison of strain and
10 classic experimental modal analysis. *Journal of Vibration and Control*,
11 22(2):371–381, 2016.
12
13
14
15 [16] D. Rovšček, J. Slavič, and M. Boltežar. The use of strain sensors in an
16 experimental modal analysis of small and light structures with free-free
17 boundary conditions. *Journal of Vibration and Control*, 19(7):1072–
18 1079, 2013.
19
20
21
22
23 [17] R. J. Wang and D. G. Shang. Fatigue life prediction based on natural
24 frequency changes for spot welds under random loading. *International*
25 *Journal of Fatigue*, 31(2):361–366, 2009.
26
27
28
29 [18] K. Shin and J. K. Hammond. *Fundamentals of signal processing*. John
30 Wiley & Sons, Ltd, Chichester, West Sussex, UK, 2008.
31
32
33
34 [19] C. Braccesi and F. Cianetti. A procedure for the virtual evaluation of the
35 stress state of mechanical system and components for automotive indus-
36 try: development and experimental validation. *Journal of Automobile*
37 *Engineering*, 219(5):633–643, 2005.
38
39
40
41 [20] C. Braccesi, F. Cianetti, G. Lori, and D. Pioli. Random multi-axial
42 fatigue: A comparative analysis among selected frequency and time
43 domain fatigue evaluation methods. *International Journal of Fatigue*,
44 74:108–118, 2015.
45
46
47
48 [21] C. Braccesi, F. Cianetti, and L. Landi. Random loads fatigue: The
49 use of spectral methods within multibody simulation. In *Proceedings of*
50 *IDETC/CIE 2005*, Long Beach, California, 2005.
51
52
53
54
55
56
57
58

- 1
2
3
4
5
6
7
8
9 [22] D. Benasciutti, F. Sherratt, and A. Cristofori. Recent developments in
10 frequency domain multi-axial fatigue analysis. *International Journal of*
11 *Fatigue*, 91:397–413, 2016.
12
13
14
15 [23] X. Pitoiset and A. Premount. Spectral methods for multi-axial random
16 fatigue analysis of metallic structure. *International Journal of Fatigue*,
17 22(7):541–550, 2000.
18
19
20
21
22 [24] G. Allegri and X. Zang. On the inverse power laws for accelerated
23 random fatigue testing. *International Journal of Fatigue*, 30(6):967–
24 977, 2008.
25
26
27
28 [25] O. H. Basquin. The exponential law of endurance tests. *American*
29 *Society of Testing Materials*, 10:625–630, 1910.
30
31
32
33 [26] D. P. Kihl, S. Sarkani, and J. E. Beach. Stochastic fatigue damage accu-
34 mulation under broadband loadings. *International Journal of Fatigue*,
35 17(5):321–329, 1995.
36
37
38
39 [27] L. Yu, P. K. Das, and D. P. Barltrop. A new look at the effect of
40 bandwidth and non-normality on fatigue damage. *Fatigue and Fracture*
41 *of Engineering Materials and Structures*, 27(1):51–58, 2004.
42
43
44
45 [28] M. Česnik and J. Slavič. Vibrational fatigue and structural dynamics
46 for harmonic and random loads. *Journal of Mechanical Engineering*,
47 60(5):339–348, 2014.
48
49
50
51 [29] M. Česnik, J. Slavič, and M. Boltežar. Uninterrupted and accelerated
52 vibrational fatigue testing with simultaneous monitoring of the natural
53
54
55
56
57
58

1
2
3
4
5
6
7
8
9 frequency and damping. *Journal of Sound and Vibration*, 331(24):5370–
10 5382, 2012.

11
12
13
14 [30] M. Mršnik, J. Slavič, and M. Boltežar. Multiaxial vibration fatiguea the-
15 oretical and experimental comparison. *Mechanical Systems and Signal*
16 *Processing*, 76:409–423, 2016.

17
18
19
20 [31] S. Winterstein. Nonlinear vibration models for extremes and fatigue.
21 *Journal of Engineering Mechanics*, 114(10):1772–1790, 1988.

22
23
24
25 [32] D. O. Smallwood. Generating non-gaussian vibration for testing pur-
26 poses. *Sound & Vibration*, 39(10):18–24, 2005.

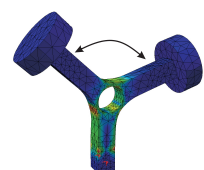
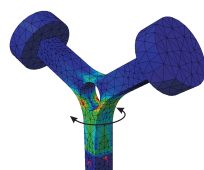
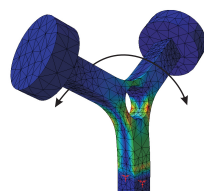
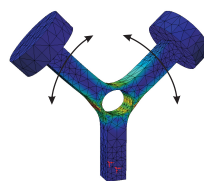
1
2
3
4
5
6
7
8
9
10
11
12
13
14
15
16
17
18
19
20
21
22
23
24
25
26
27
28
29
30
31
32
33
34
35
36
37
38
39
40
41
42
43
44
45
46
47
48
49
50
51
52
53
54
55
56
57
58
59
60
61
62
63
64
65

List of Tables

1	Y-specimen's natural frequencies with corresponding mode-	
	shapes.	32
2	Input loadings characteristics	33
3	Comparison between actual and estimated fatigue life	34
4	Output Kurtosis of The Stress Time Histories	35
5	Results obtained by adoption of non-Gaussianity coefficient [14]	36

1
2
3
4
5
6
7
8
9
10
11
12
13
14
15
16
17
18
19
20
21
22
23
24
25
26
27
28
29
30
31
32
33
34
35
36
37
38
39
40
41
42
43
44
45
46
47
48
49
50
51
52
53
54
55
56
57
58
59
60
61
62
63
64
65

Table 1: Y-specimen's natural frequencies with corresponding modeshapes.

Nr.	Natural frequency/ Modeshape
1.	$\omega_1 = 290$ Hz 
2.	$\omega_2 = 344$ Hz 
3.	$\omega_3 = 425$ Hz 
4.	$\omega_4 = 775$ Hz 

1
2
3
4
5
6
7
8
9
10
11
12
13
14
15
16
17
18
19
20
21
22
23
24
25
26
27
28
29
30
31
32
33
34
35
36
37
38
39
40
41
42
43
44
45
46
47
48
49
50
51
52
53
54
55
56
57
58
59
60
61
62
63
64
65

Table 2: Input loadings characteristics

<i>Nr.</i>	<i>Signal</i>	k_u	s_k
1.	<i>Gaussian</i>	2.96	1.76×10^{-5}
2.	<i>Stationary non-Gaussian</i>	7.36	-0.0345
3.	<i>Stationary non-Gaussian</i>	5.43	-1.210^{-5}
4.	<i>non-Stationary non-Gaussian</i>	7.08	4.21×10^{-6}

1
2
3
4
5
6
7
8
9
10
11
12
13
14
15
16
17
18
19
20
21
22
23
24
25
26
27
28
29
30
31
32
33
34
35
36
37
38
39
40
41
42
43
44
45
46
47
48
49
50
51
52
53
54
55
56
57
58
59
60
61
62
63
64
65

Table 3: Comparison between actual and estimated fatigue life

<i>Specimen</i>	<i>PSD Level</i>	<i>Input</i>	<i>Actual Life</i>	<i>Estimated Life</i>
	$[N^2/Hz]$	k_u	$[s]$	$[s]$
1	15.5	2.96	1115	1239.9
2	15.5	2.96	783	1239.9
3	12	2.96	9313	12429
4	8	2.96	70564	90500
5	15.5	7.36	1248	1255.2
6	12	7.36	4704	12975
7	8	7.36	76981	81654
8	15.5	5.43	1433	1094.2
9	12	5.43	1713	5934.5
10	8	5.43	71695	76563
11	15.5	7.08	302	1030.6
12	12	7.08	604	1343.7
13	8	7.08	1359	91710

1
2
3
4
5
6
7
8
9
10
11
12
13
14
15
16
17
18
19
20
21
22
23
24
25
26
27
28
29
30
31
32
33
34
35
36
37
38
39
40
41
42
43
44
45
46
47
48
49
50
51
52
53
54
55
56
57
58
59
60
61
62
63
64
65

Table 4: Output Kurtosis of The Stress Time Histories

<i>Signal</i>	<i>Input</i>	<i>Actual Output</i>	<i>Estimated Output</i>
	k_u	k_u	k_u
<i>Stationary</i>	7.36	2.85	3.26
<i>Stationary</i>	5.43	2.78	3.05
<i>non-Stationary(Burst)</i>	7.08	6.08	6.55

1
2
3
4
5
6
7
8
9
10
11
12
13
14
15
16
17
18
19
20
21
22
23
24
25
26
27
28
29
30
31
32
33
34
35
36
37
38
39
40
41
42
43
44
45
46
47
48
49
50
51
52
53
54
55
56
57
58
59
60
61
62
63
64
65

Table 5: Results obtained by adoption of non-Gaussianity coefficient [14]

<i>Signal</i>	<i>Output</i> k_u	<i>Correction</i> <i>coefficient</i>	<i>Correctly Estimated</i> <i>Life[s]</i>	<i>Actual</i> <i>Life[s]</i>
<i>Stationary</i>	2.85	0.98	1277.1	1248
<i>Stationary</i>	2.78	1.07	1021.4	1433
<i>non-Stationary(burst)</i>	6.08	20.54	655	302

1
2
3
4
5
6
7
8
9
10
11
12
13
14
15
16
17
18
19
20
21
22
23
24
25
26
27
28
29
30
31
32
33
34
35
36
37
38
39
40
41
42
43
44
45
46
47
48
49
50
51
52
53
54
55
56
57
58
59
60
61
62
63
64
65

List of Figures

1	Fixed Y-shaped specimen.	38
2	Theoretical Input PSD	39
3	Input loadings: (a) Stationary $k_u = 3$. (b) Stationary $k_u = 7$. (c) Stationary $k_u = 5.5$. (d) non-Stationary $k_u = 7$	40
4	FEM model of the specimen.	41
5	Comparison between numerically and experimentally obtained response acceleration PSD	42
6	Frequency shift of the observed natural frequency.	43
7	Experimental and calculated fatigue lives.	44
8	Experimental fatigue lives.	45
9	Corrected fatigue lives.	46

1
2
3
4
5
6
7
8
9
10
11
12
13
14
15
16
17
18
19
20
21
22
23
24
25
26
27
28
29
30
31
32
33
34
35
36
37
38
39
40
41
42
43
44
45
46
47
48
49
50
51
52
53
54
55
56
57
58
59
60
61
62
63
64
65

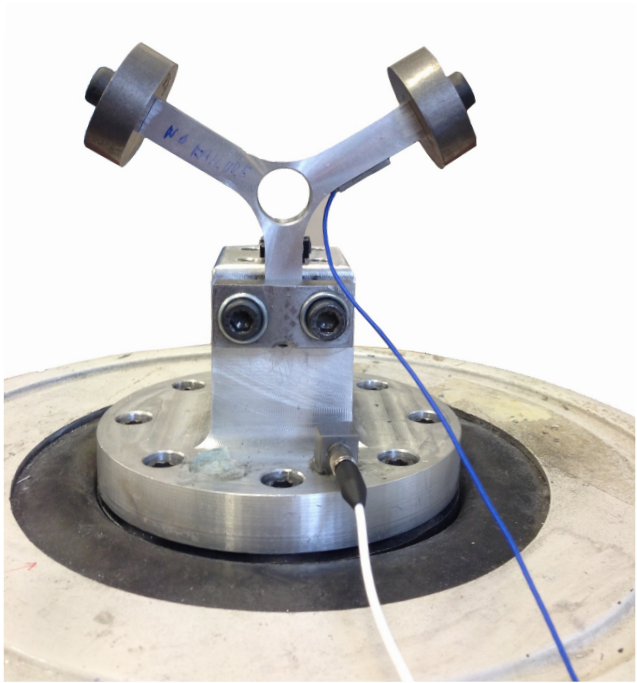


Figure 1: Fixed Y-shaped specimen.

1
2
3
4
5
6
7
8
9
10
11
12
13
14
15
16
17
18
19
20
21
22
23
24
25
26
27
28
29
30
31
32
33
34
35
36
37
38
39
40
41
42
43
44
45
46
47
48
49
50
51
52
53
54
55
56
57
58
59
60
61
62
63
64
65

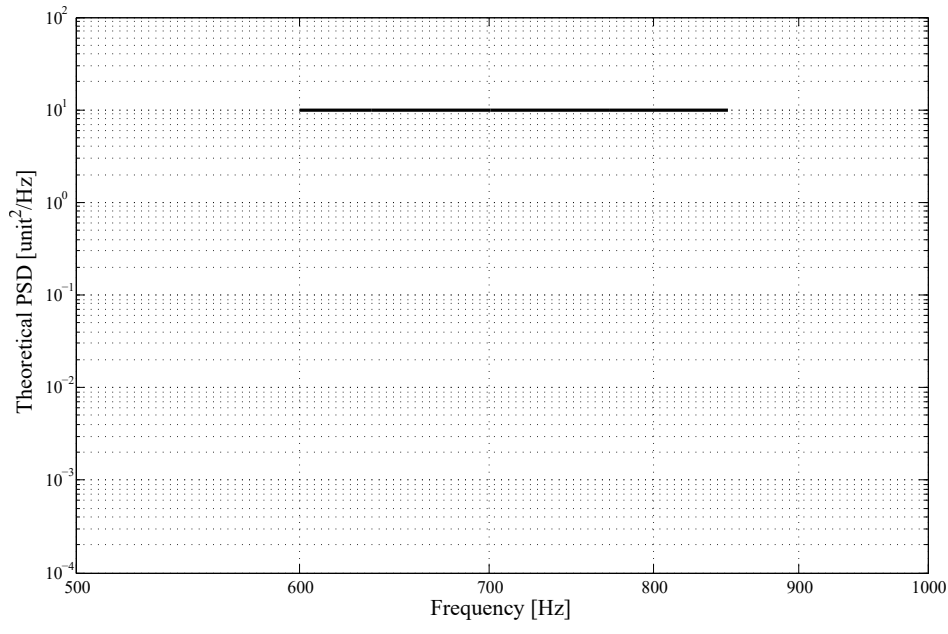


Figure 2: Theoretical Input PSD

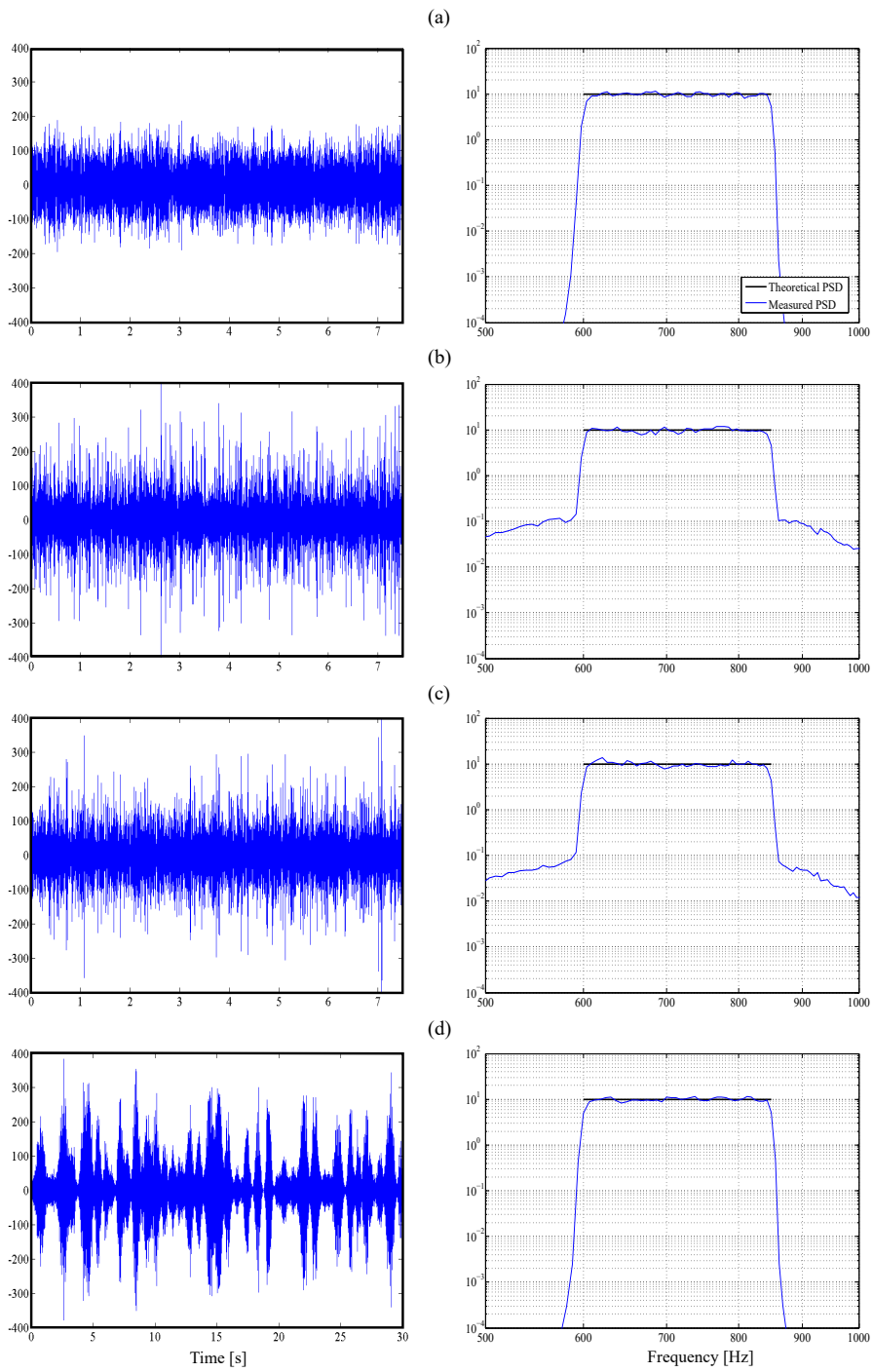


Figure 3: Input loadings: (a) Stationary $k_u = 3$. (b) Stationary $k_u = 7$. (c) Stationary $k_u = 5.5$. (d) non-Stationary $k_u = 7$

1
2
3
4
5
6
7
8
9
10
11
12
13
14
15
16
17
18
19
20
21
22
23
24
25
26
27
28
29
30
31
32
33
34
35
36
37
38
39
40
41
42
43
44
45
46
47
48
49
50
51
52
53
54
55
56
57
58
59
60
61
62
63
64
65

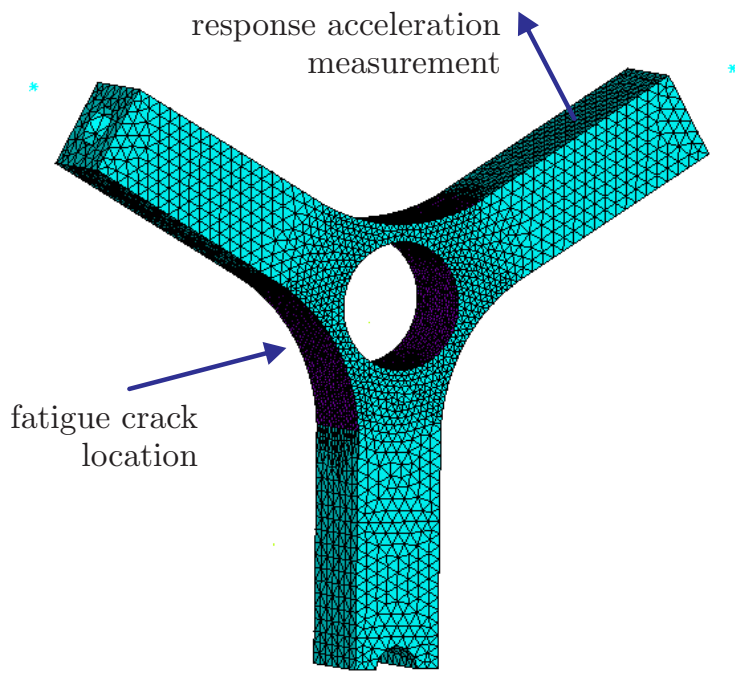


Figure 4: FEM model of the specimen.

1
2
3
4
5
6
7
8
9
10
11
12
13
14
15
16
17
18
19
20
21
22
23
24
25
26
27
28
29
30
31
32
33
34
35
36
37
38
39
40
41
42
43
44
45
46
47
48
49
50
51
52
53
54
55
56
57
58
59
60
61
62
63
64
65

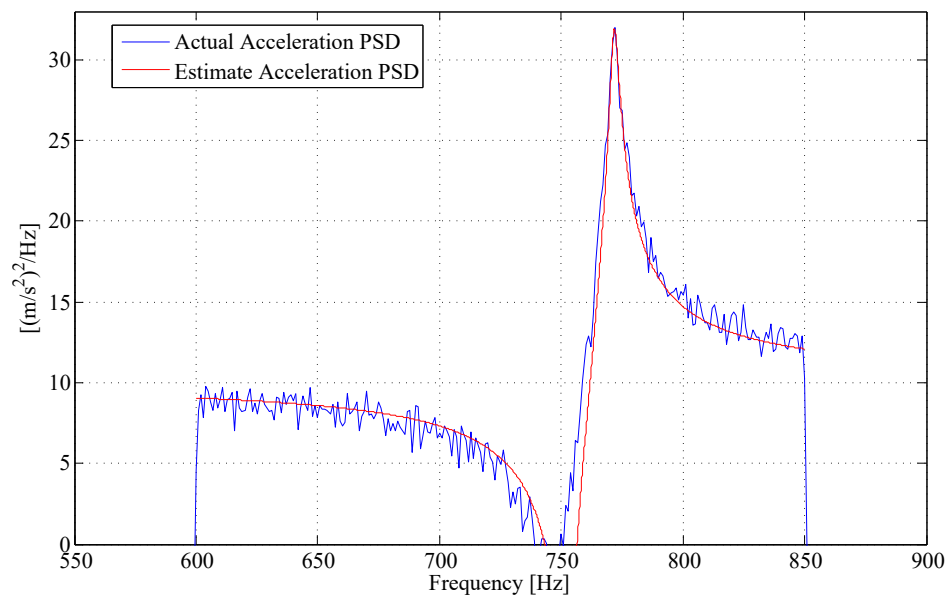


Figure 5: Comparison between numerically and experimentally obtained response acceleration PSD

1
2
3
4
5
6
7
8
9
10
11
12
13
14
15
16
17
18
19
20
21
22
23
24
25
26
27
28
29
30
31
32
33
34
35
36
37
38
39
40
41
42
43
44
45
46
47
48
49
50
51
52
53
54
55
56
57
58
59
60
61
62
63
64
65

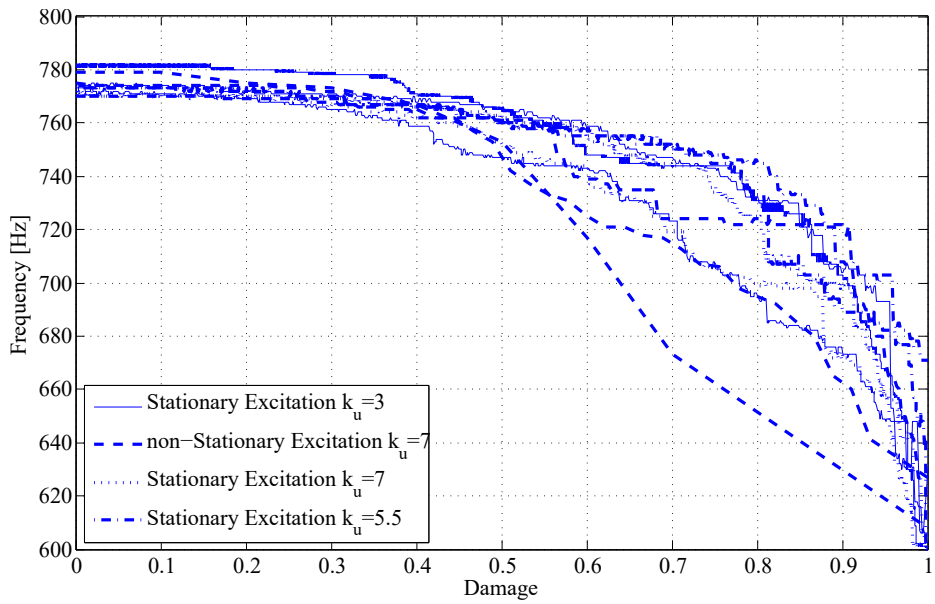


Figure 6: Frequency shift of the observed natural frequency.

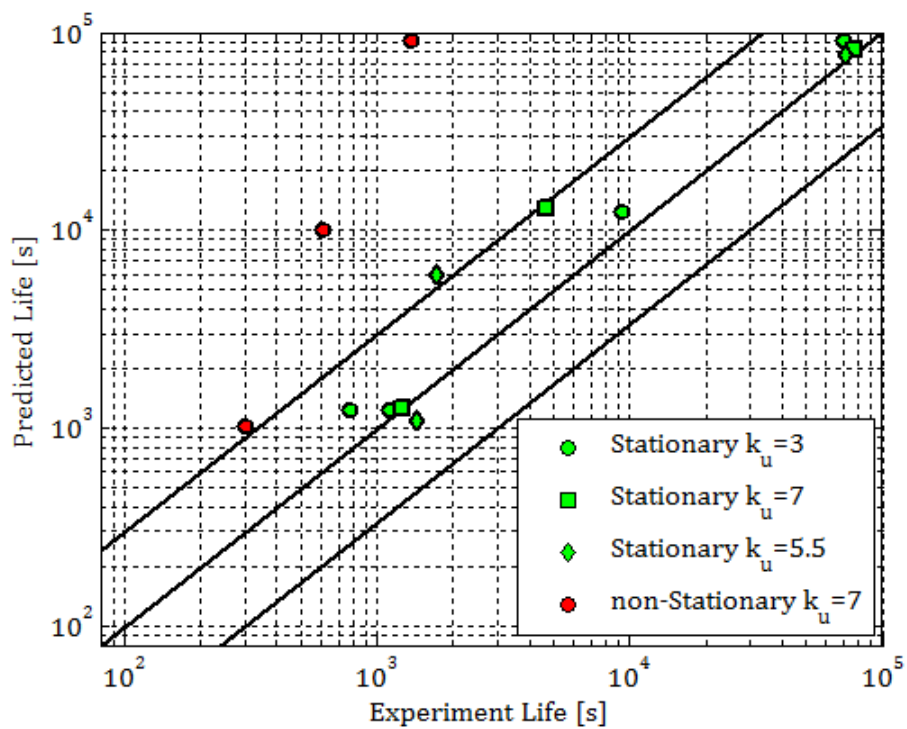


Figure 7: Experimental and calculated fatigue lives.

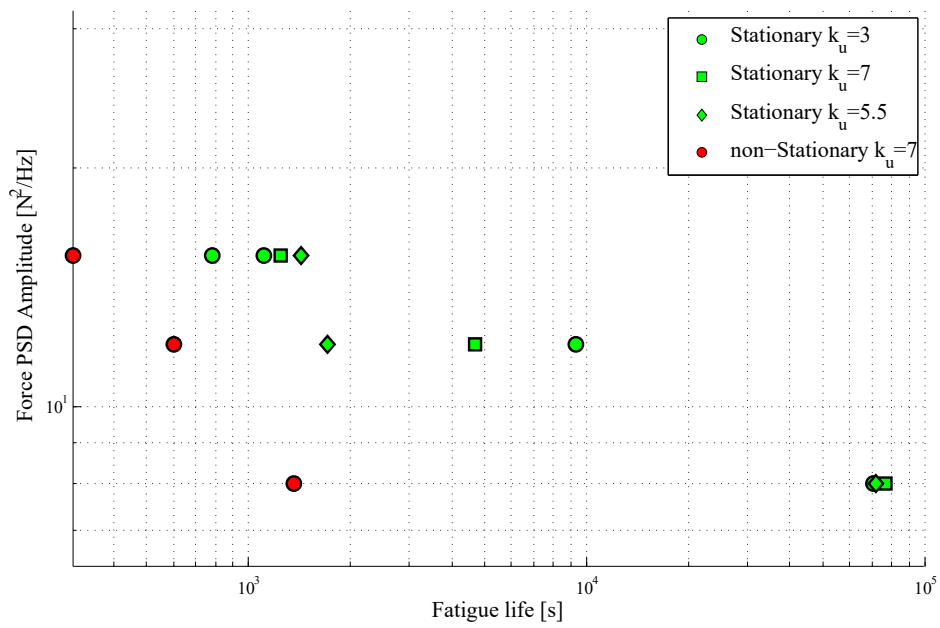


Figure 8: Experimental fatigue lives.

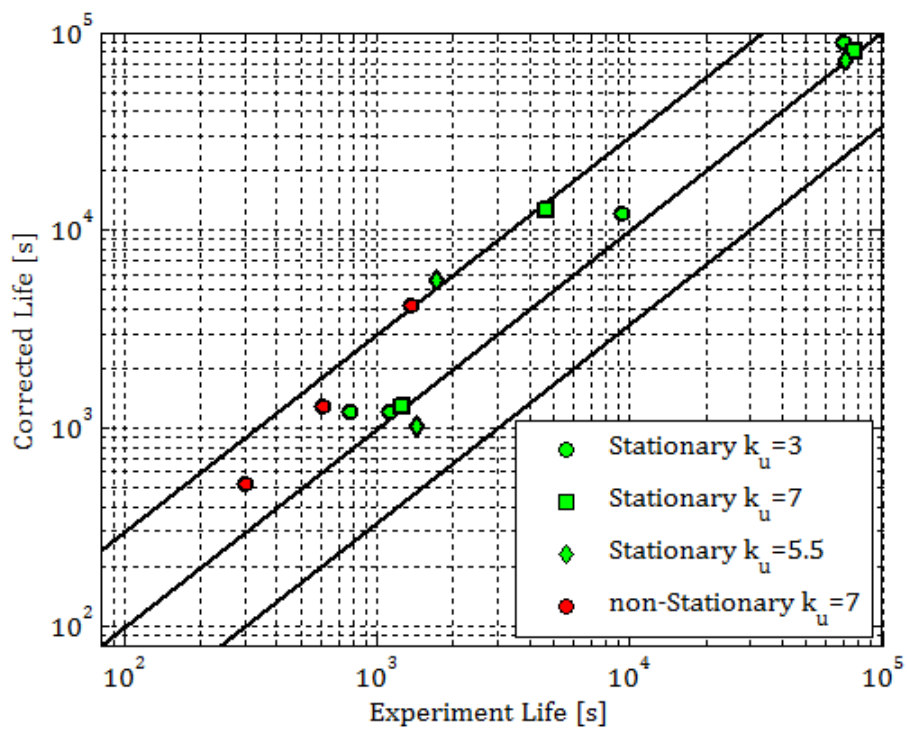


Figure 9: Corrected fatigue lives.